HAPLESS13, the Arabidopsis μ1 Adaptin, Is Essential for Protein Sorting at the trans-Golgi Network/Early Endosome[1][C][W][OPEN]

Jia-Gang Wang[2], Sha Li[2], Xin-Ying Zhao, Liang-Zi Zhou, Guo-Qiang Huang, Chong Feng, and Yan Zhang*

State Key Laboratory of Crop Biology, College of Life Sciences, Shandong Agricultural University, Tai'an 271018, China

ORCID ID: 0000-0002-3501-5857 (Y.Z.).

In plant cells, secretory and endocytic routes intersect at the trans-Golgi network (TGN)/early endosome (EE), where cargos are further sorted correctly and in a timely manner. Cargo sorting is essential for plant survival and therefore necessitates complex molecular machinery. Adaptor proteins (APs) play key roles in this process by recruiting coat proteins and selecting cargos for different vesicle carriers. The μ1 subunit of AP-1 in Arabidopsis (*Arabidopsis thaliana*) was recently identified at the TGN/EE and shown to be essential for cytokinesis. However, little was known about other cellular activities affected by mutations in AP-1 or the developmental consequences of such mutations. We report here that HAPLESS13 (HAP13), the Arabidopsis μ1 adaptin, is essential for protein sorting at the TGN/EE. Functional loss of *HAP13* displayed pleiotropic developmental defects, some of which were suggestive of disrupted auxin signaling. Consistent with this, the asymmetric localization of PIN-FORMED2 (PIN2), an auxin transporter, was compromised in the mutant. In addition, cell morphogenesis was disrupted. We further demonstrate that HAP13 is critical for brefeldin A-sensitive but wortmannin-insensitive post-Golgi trafficking. Our results show that HAP13 is a key link in the sophisticated trafficking network in plant cells.

Plant cells contain sophisticated endomembrane compartments, including the endoplasmic reticulum, the Golgi, the trans-Golgi network (TGN)/early endosome (EE), the prevacuolar compartments/multivesicular bodies (PVC/MVB), various types of vesicles, and the plasma membrane (PM; Ebine and Ueda, 2009; Richter et al., 2009). Intracellular protein sorting between the various locations in the endomembrane system occurs in both secretory and endocytic routes (Richter et al., 2009; De Marcos Lousa et al., 2012). Vesicles in the secretory route start at the endoplasmic reticulum, passing through the Golgi before reaching the TGN/EE, while vesicles in the endocytic route start from the PM before reaching the TGN/EE (Dhonukshe et al., 2007; Viotti et al., 2010). The TGN/EE in Arabidopsis (*Arabidopsis thaliana*) is an independent and highly dynamic organelle transiently associated with the Golgi (Dettmer et al., 2006; Lam et al., 2007; Viotti et al., 2010), distinct from the animal TGN. Once reaching the TGN/EE, proteins delivered by their vesicle carriers are subject to further sorting, being incorporated either into vesicles that pass through the PVC/MVB before reaching the vacuole for degradation or into vesicles that enter the secretory pathway for delivery to the PM (Ebine and Ueda, 2009; Richter et al., 2009). Therefore, the TGN/EE is a critical sorting compartment that lies at the intersection of the secretory and endocytic routes.

Fine-tuned control of intracellular protein sorting at the TGN/EE is essential for plant development (Geldner et al., 2003; Dhonukshe et al., 2007, 2008; Richter et al., 2007; Kitakura et al., 2011; Wang et al., 2013). An auxin gradient is crucial for pattern formation in plants, whose dynamic maintenance requires the polar localization of auxin efflux carrier PINs through endocytic recycling (Geldner et al., 2003; Blilou et al., 2005; Paciorek et al., 2005; Abas et al., 2006; Jaillais et al., 2006; Dhonukshe et al., 2007; Kleine-Vehn et al., 2008). Receptor-like kinases (RLKs) have also been recognized as major cargos undergoing endocytic trafficking, which are either recycled back to the PM or sent for vacuolar degradation (Geldner and Robatzek, 2008; Irani and Russinova, 2009). RLKs are involved in most if not all developmental processes of plants (De Smet et al., 2009).

Intracellular protein sorting relies on sorting signals within cargo proteins and on the molecular machinery that recognizes sorting signals (Boehm and Bonifacino, 2001; Robinson, 2004; Dhonukshe et al., 2007). Adaptor proteins (AP) play a key role (Boehm and Bonifacino, 2001; Robinson, 2004) in the recognition of sorting

---

signals. APs are heterotetrameric protein complexes composed of two large subunits (β and $\gamma/\alpha/\delta/\varepsilon$), a small subunit ($\sigma$), and a medium subunit (μ) that is crucial for cargo selection (Boehm and Bonifacino, 2001). APs associate with the cytoplasmic side of secretory and endocytic vesicles, recruiting coat proteins and recognizing sorting signals within cargo proteins for their incorporation into vesicle carriers (Boehm and Bonifacino, 2001). Five APs have been identified so far, classified by their components, subcellular localization, and function (Boehm and Bonifacino, 2001; Robinson, 2004; Hirst et al., 2011). Of the five APs, AP-1 associates with the TGN or recycling endosomes (RE) in yeast and mammals (Huang et al., 2001; Robinson, 2004), mediating the sorting of cargo proteins to compartments of the endosomal-lysosomal system or to the basolateral PM of polarized epithelial cells (Gonzalez and Rodriguez-Boulan, 2009). Knockouts of AP-1 components in multicellular organisms resulted in embryonic lethality (Boehm and Bonifacino, 2001; Robinson, 2004).

We show here that the recently identified Arabidopsis μ1 adaptin AP1M2 (Park et al., 2013; Teh et al., 2013) is a key component in the cellular machinery mediating intracellular protein sorting at the TGN/EE. AP1M2 was previously named *HAPLESS13* (*HAP13*), whose mutant allele *hap13* showed male gametophytic lethality (Johnson et al., 2004). In recent quests for AP-1 in plants, HAP13/AP1M2 was confirmed as the Arabidopsis μ1 adaptin based on its interaction with other components of the AP-1 complex as well as its localization at the TGN (Park et al., 2013; Teh et al., 2013). A novel mutant allele of *HAP13/AP1M2*, *ap1m2-1*, was found to be defective in the intracellular distribution of KNOLLE, leading to defective cytokinesis (Park et al., 2013; Teh et al., 2013). However, it was not clear whether HAP13/AP1M2 mediated other cellular activities and their developmental consequences. Using the same mutant allele, we found that functional loss of *HAP13* (*hap13-1/ap1m2-1*) resulted in a full spectrum of growth defects, suggestive of compromised auxin signaling and of defective RLK signaling. Cell morphogenesis was also disturbed in *hap13-1*. Importantly, *hap13-1* was insensitive to brefeldin A (BFA) washout, indicative of defects in guanine nucleotide exchange factors for ADP-ribosylation factor (ArfGEF)-mediated post-Golgi trafficking. Furthermore, HAP13/AP1M2 showed evolutionarily conserved function during vacuolar fusion, providing additional support to its identity as a μ1 adaptin. These results demonstrate the importance of the Arabidopsis μ1 adaptin for intracellular protein sorting centered on the TGN/EE.

RESULTS

HAP13 Is Constitutively Expressed and Critical for Plant Growth

To determine the expression pattern of *HAP13*, we generated Pro_{HAP13}:*GUS* reporter lines and found out that *HAP13* is expressed in all tissues throughout developmental stages (Supplemental Methods S1), including seedlings (Fig. 1A), leaves (Fig. 1, B and C), roots (Fig. 1D), and reproductive organs (Fig. 1, E–H) as well as in various cell types such as root hairs (Fig. 1I), trichomes (Fig. 1J), pollen (Fig. 1K), and growing pollen tubes (Fig. 1L), suggesting its function beyond the gametophytic stage.

To determine the function of *HAP13* in sporophytic tissues, we characterized an additional allele of *HAP13* (Fig. 2A) and confirmed that no full-length transcript of *HAP13* could be detected in *hap13-1/ap1m2-1* (Teh et al., 2013; Supplemental Methods S1). However, a partial transcript potentially encoding a truncated HAP13 with the first 229 amino acids (HAP13$_{N229}$) was detected in *hap13-1*. This truncated protein would be able to incorporate into the AP-1 complex but unable to interact with cargo proteins according to the structure of its homologs in metazoa (Heldwein et al., 2004). Homozygous *hap13-1* plants were obtained at a significantly distorted ratio (Supplemental Table S1) due to defective male gametophytic function (Supplemental Fig. S1). *hap13-1* showed pleiotropic developmental defects (Fig. 2, C–G). The growth of primary roots of *hap13-1* arrested precociously (Fig. 2C; Supplemental Fig. S2A), whereas the number of lateral roots increased significantly (Fig. 2, D and E; Supplemental Fig. S2B). Wild-type plants grown in soil for 30 to 35 d started the reproductive phase (Fig. 2F), whereas *hap13-1* hardly made the transition to reproductive growth when grown in soil (Fig. 2G), although it did manage to produce inflorescences when maintained on Murashige and Skoog (MS) medium in sterile glass tubes (Fig. 2, L–O). Compared with the wild type (Fig. 2H), *hap13-1* had compacted inflorescences due to less elongated pedicles (Fig. 2M). All four whorls were present but were much smaller in *hap13-1* (Fig. 2, L–O) than in the wild type (Fig. 2, I–K). Sepals, petals, and pistils were deformed in *hap13-1*, showing uneven surfaces, loss of conical cell shape, and non-elongating papilla cells, respectively (Fig. 2, L, N, and O). Because *hap13-1* showed early senescence, we analyzed reactive oxygen species (ROS) levels and cell death. Indeed, compared with the wild type at the same developmental stages, both ROS production and cell death were increased in *hap13-1* (Supplemental Fig. S3). ROS production was higher in newly initiated rather than old *hap13-1* leaves, whereas cell death was more severe in older true leaves than in cotyledons or newly initiated leaves of *hap13-1* (Supplemental Fig. S3).

HAP13 Is Essential for Vascular Development

That *HAP13* expression was detected in vascular tissues throughout development (Fig. 1) and *hap13-1* displayed defective organ formation (Fig. 2) suggested that *HAP13* was essential for vascular development. To test this hypothesis, we characterized the vasculature of leaves, roots, hypocotyls, and stems (Fig. 3). The leaf venation network of *hap13-1* was different from that of the wild type in three
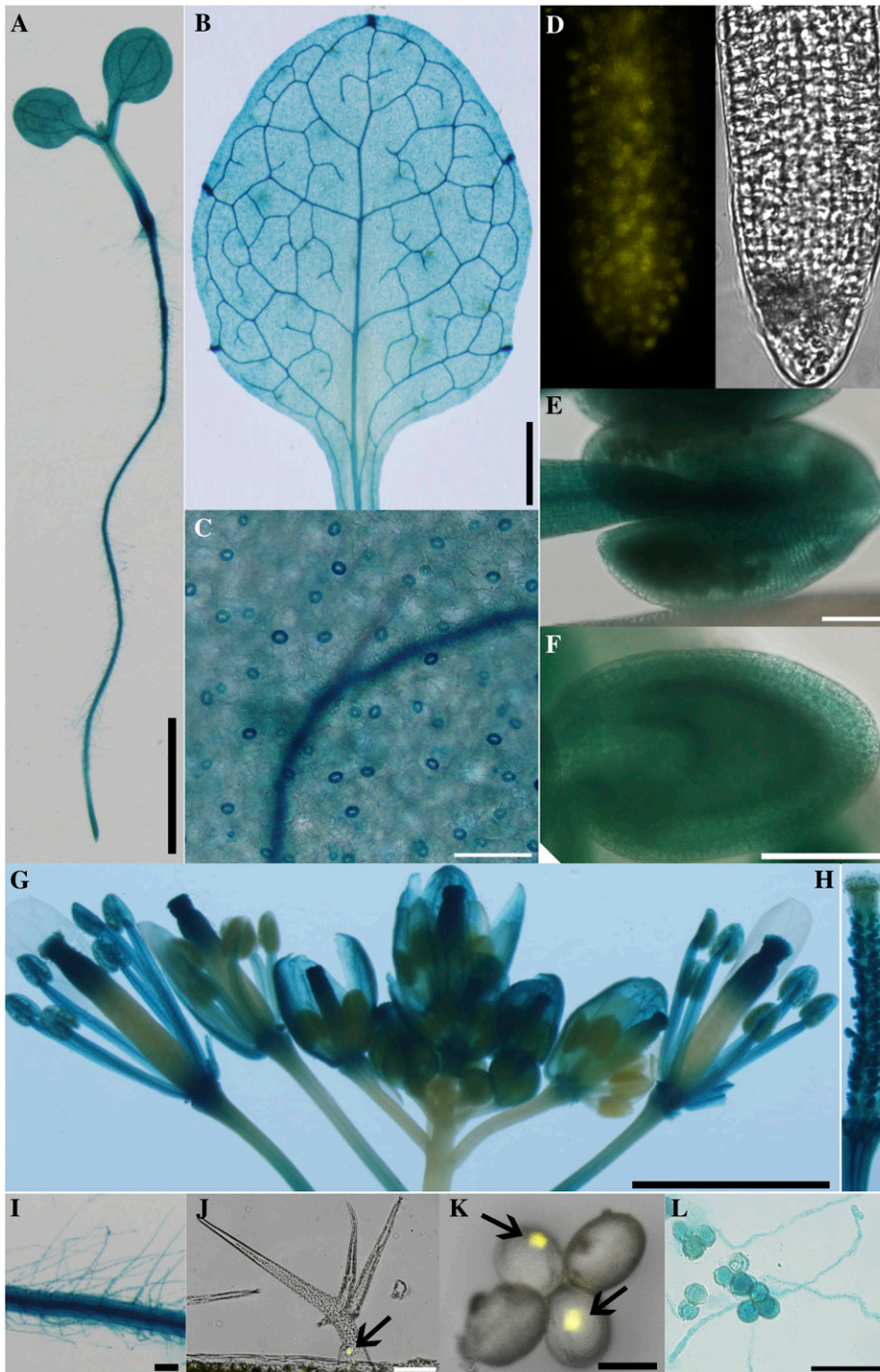
Figure 1. *HAP13* is widely expressed. Representative images from 20 individual transgenic lines expressing *Pro_HAP13*:GUS (A–C, E–I, and L) or from six individual transgenic lines of *Pro_HAP13*:NLS-YFP (D, J, and K) are shown: 4-DAG seedling (A), leaf from 20-DAG plants (B), epidermal cells (C), root (D), developing anther (E), developing seed (F), inflorescence (G), mature pistil (H), root hairs (I), trichomes (J), pollen grains (K), and growing pollen tubes (L). Bars = 2 mm for A, B, and G, 100 μm for C to F, I, J, and L, 500 μm for H, and 20 μm for K.

aspects (Fig. 3, A and B). First, in contrast to the closed loops of the wild type (Fig. 3A), *hap13-1* had incomplete loops such that all distal veins were open (Fig. 3B). Second, higher order veins present in the wild type (Fig. 3A; i.e. tertiary and quaternary veins) were absent in *hap13-1* (Fig. 3B). Third, vascular islands, veins broken from the venation network, were detected in *hap13-1* leaves (Fig. 3B). To determine whether

these venation defects were due to defects in procambial formation or differentiation, we introduced the procambial marker *Pro_HB8*:GUS (Cnops et al., 2006) into *hap13-1*. Similar venation defects were observed after staining for GUS, including highly reduced venation complexity, incomplete loops, as well as vascular islands (Supplemental Fig. S4), suggesting that both procambial patterning and differentiation were

Figure 2. Characterization of *hap13-1*. A and B, Schematic illustration of *HAP13* genomic organization and transcript analysis of the insertional mutants. "Comp" indicates the *HAP13-GFP;hap13-1* plants. WT, Wild type. C, Wild-type (left) and *hap13-1* (right) seedlings at 7 DAG. D and E, A *hap13-1* plant on MS medium at 20 DAG (D) or 30 DAG (E). F and G, Wild type (F) and *hap13-1* (G) plants grown in soil at 40 DAG. The image shown in G was taken at the same scale as that shown in F. H to K, Inflorescence (H), petal (I), sepal (J), and pistil (K) of the wild type. Sepals and petals are partially removed from two flowers in H to show the inner whorls. The inset in I shows epidermal cells of a wild-type petal. L to O, A representative pistil (L), inflorescence (M), petal (N), and sepal (O) of *hap13-1*. The inset in N shows epidermal cells of a *hap13-1* petal. Bars = 2 mm for C to E, 500 μm for H and M, 5 μm for H and M insets, 50 μm for I, J, N, and O, and 100 μm for K and L.
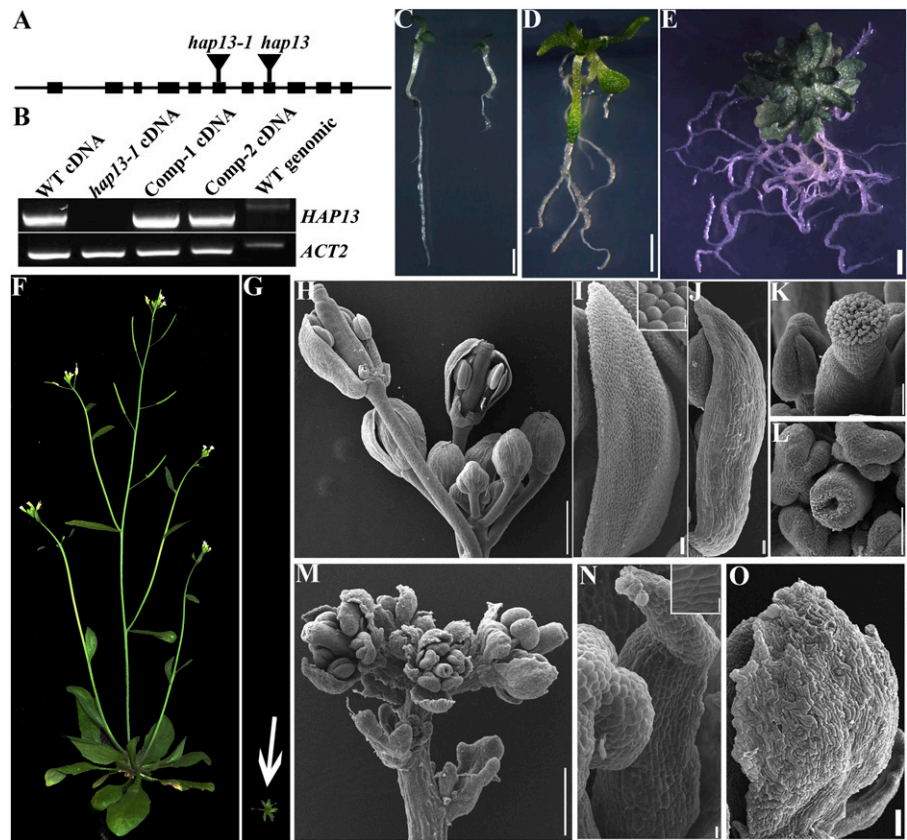
defective in *hap13-1*. Transmission electron micrography (TEM) of leaf vasculature showed that the xylem of *hap13-1* (Fig. 3D) did not form the lignified hollow tubular structure as in the wild type (Fig. 3C), indicating defective programmed cell death of xylem cells.

The vasculature of stems from just bolted plants or below the inflorescence (Altamura et al., 2001) typically contains six to eight vascular bundles that are distributed in an orderly circular way (Fig. 3, G and J), centering on heterogenous parenchyma cells (Fig. 3, G and J). Within each bundle, the phloem and the xylem are separated by a fascicular cambium that continues to differentiate into either phloem or xylem (Fig. 3, H and I). However, the ordered distribution of vascular bundles was lost in *hap13-1*, such that all vascular bundles either formed a continuous organization (Fig. 3K) or were distributed randomly within the stem (Fig. 3N). Within each discernible vascular bundle in *hap13-1*, the normal spatial distribution of phloem and xylem was disrupted (Fig. 3, L and M). In addition, both the phloem and the interfascicular cambium were hardly detected (Fig. 3M). In contrast to the absence of both phloem and interfascicular cambium, the cells of the cortex layer surrounding the vascular bundles had proliferated (Fig. 3, K–N). Despite the deformation of vascular systems in the aerial parts of *hap13-1*, the vascular development of roots and hypocotyls in *hap13-1* (Fig. 3F; Supplemental Fig. S4) was not discernibly different from that of the wild type (Fig. 3E;

Supplemental Fig. S4), indicating that *HAP13* might be essential for vascular development in the aerial parts.

Dynamic Auxin Distribution Was Compromised in *hap13-1*

The developmental defects of *hap13-1*, such as leaf morphogenesis, vascular development, as well as root growth, suggested altered auxin signaling (Abas et al., 2006; Rosado et al., 2010; Kitakura et al., 2011). To determine if auxin distribution was perturbed in *hap13-1*, we introduced the synthetic auxin response promoter Pro_{DR5} (Ulmasov et al., 1997) in *hap13-1* and analyzed the expression of GUS or GFP reporters. GUS signals were mostly restricted to the apex and slightly along the edge (Fig. 4A) of cotyledons at 6 d after germination (DAG) as well as at the primary root tips in the wild type (Fig. 4C). By contrast, ectopic GUS signals were detected at the basal parts of the *hap13-1* cotyledons (Fig. 4B). In roots, GUS signals were weak in the root tips of *hap13-1* but expanded ectopically (Fig. 4D). These expression patterns were confirmed by Pro_{DR5}:GFP; instead of the strong and spatially restricted signals in the wild type (Fig. 4G), weak but expanded GFP signals were detected in *hap13-1* (Fig. 4H), suggestive of a compromised auxin gradient in *hap13-1*. We further tested the root gravitropic response, a dynamic process regulated by auxin (Abas et al., 2006; Rosado et al., 2010; Kitakura et al., 2011).
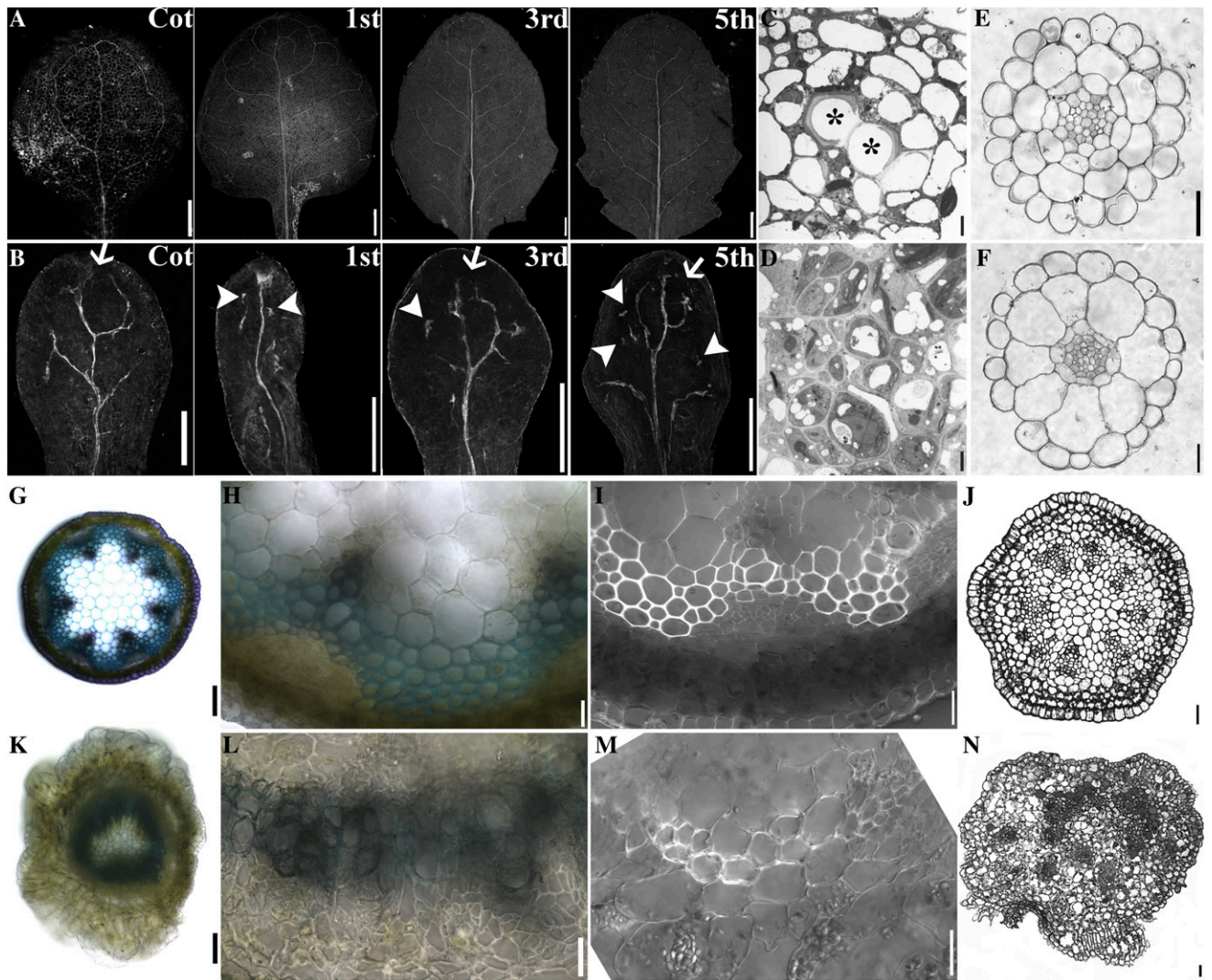
Figure 3. *HAP13* is essential for vascular development. A and B, Venation patterns of 25-DAG wild-type (A) and *hap13-1* (B) leaves. Cot is a representative of cotyledons. Other leaves were representative of first, third, and fifth true leaves. Arrows indicate open ends and arrowheads indicate vascular islands. C and D, TEM of wild-type (C) and *hap13-1* (D) leaf vasculature. Asterisks show lignified xylem cells in the wild type. E and F, Transverse sections of wild-type (E) and *hap13-1* (F) roots. G, A hand-cut section of a young stem from the wild type. H, Closeup of the section shown in G. I, A hand-cut section of a wild-type young stem. J, Transverse section of a wild-type inflorescence stem. K, A hand-cut section of a young stem from *hap13-1*. L, Closeup of the section shown in K. M, A hand-cut section of a *hap13-1* young stem. N, A transverse section of a *hap13-1* inflorescence stem. Bars = 2 mm for A and B, 20 μm for C, D, H to J, and L to N, 2 μm for E and F, and 100 μm for G and K.

Indeed, roots of *hap13-1* were less responsive to gravity (Fig. 4K). The hyposensitivity of *hap13-1* to gravity was confirmed by histochemical analysis of Pro_{DR5}:GUS; *hap13-1* (Fig. 4, E and F). In addition, columena cells that sense gravity were ordered in the wild type (Fig. 4I) but disorganized in *hap13-1* (Fig. 4J). These results suggested compromised auxin distribution in *hap13-1*.

HAP13 Is Critical for Cell Morphogenesis

Because *HAP13* is expressed in most, if not all, cell types (Fig. 1), we asked if cell morphogenesis was affected in *hap13-1*. Wild-type leaves were flat and

symmetric (Fig. 5A). By contrast, *hap13-1* leaves were rugged and asymmetric (Fig. 5B). Leaf pavement cells were significantly smaller and lost their characteristic jigsaw puzzle shape in *hap13-1* (Fig. 5, C, D, K, and L). Trichomes are less complex in *hap13-1*; most trichomes on *hap13-1* leaves showed only one branch (Fig. 5, F and M), while three branches were typical on the wild type (Fig. 5, E and M). Defects in cell morphogenesis in *hap13-1* extended to the epidermal and cortex cells in roots and hypocotyls (Fig. 5H; Supplemental Fig. S4). The wild type showed rectangle-shaped epidermal or cortex cells from longitudinal growth, whereas the growth polarity of *hap13-1* cells was disrupted, leading

Figure 4. Auxin distribution and responses are compromised in *hap13-1*. A to F, GUS staining of 6-DAG seedlings of *Pro_DR5*:GUS (A, C, and E) and *Pro_DR5*:GUS;*hap13-1* (B, D, and F). Roots were turned at a 135° angle for 6 h for E and F. Representative images of 36 seedlings from three batches are shown. Arrows indicate ectopic GUS signals, and arrowheads indicate the region where GUS signal was redistributed during gravitropism. G and H, Primary root tips labeled with FM4-64 from 6-DAG *Pro_DR5*:GFP (G) or *Pro_DR5*: GFP;*hap13-1* (H). I and J, Lugol's staining of primary root tip from 6-DAG Ws (I) or *hap13-1* (J). K, Curvature of a primary root tip after a 135° turning at various time points. Data were collected from three independent experiments, with 36 seedlings for each genetic background. Results shown in K are given as means ± SE. The gravitropic response between Ws and *hap13-1* was significantly different (Student's *t* test, $P < 0.01$). Bars = 500 μm for A and B, 200 μm for C to F, I, and J, and 25 μm for G and H.
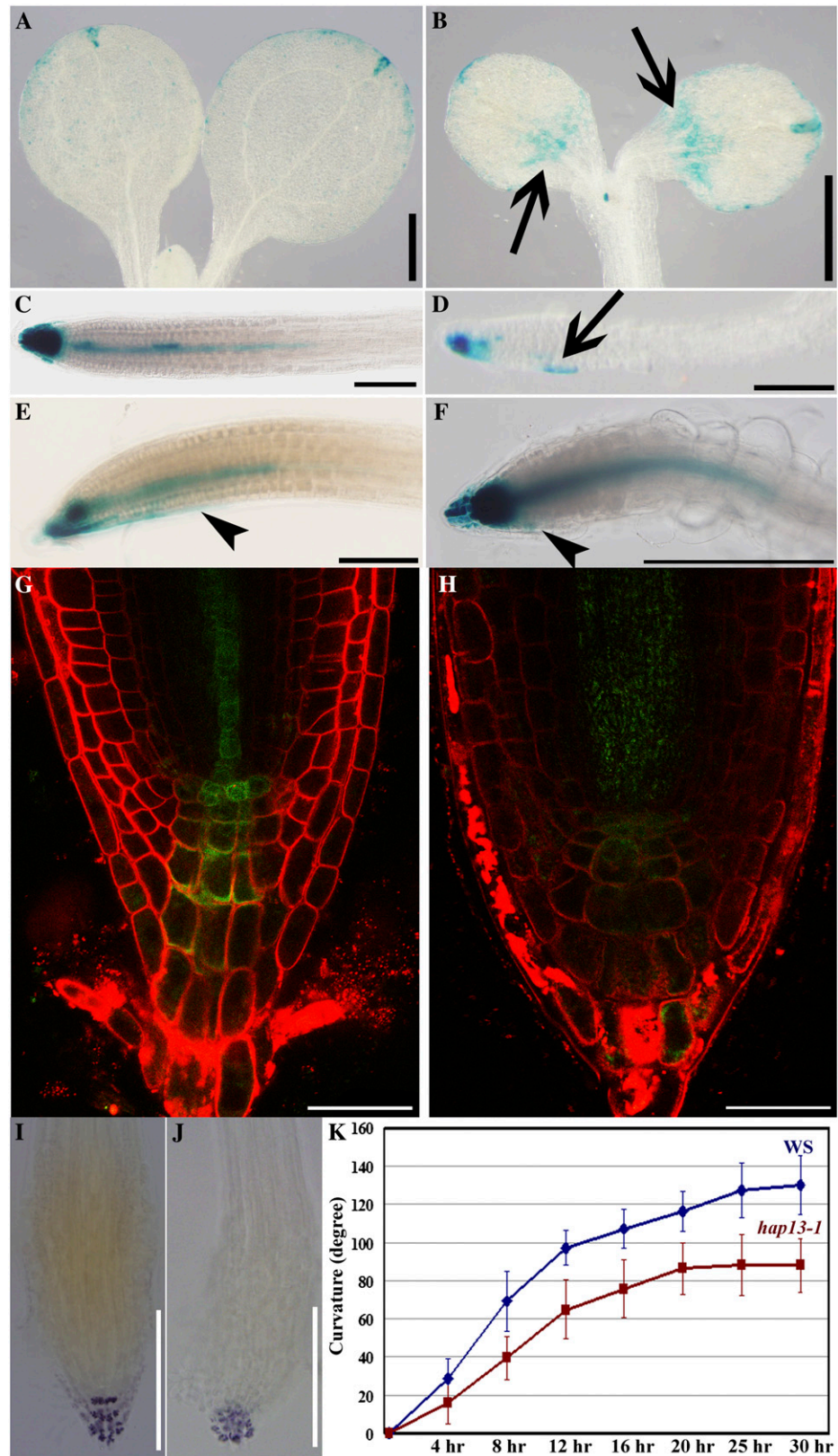
to irregularly shaped or ballooning cells (Fig. 5H; Supplemental Fig. S4). Root hairs, the other tip-growing cells in addition to pollen tubes, were either bulged or hardly initiated in *hap13-1* (Fig. 5J), further demonstrating the importance of *HAP13* in cell polarity and morphogenesis.
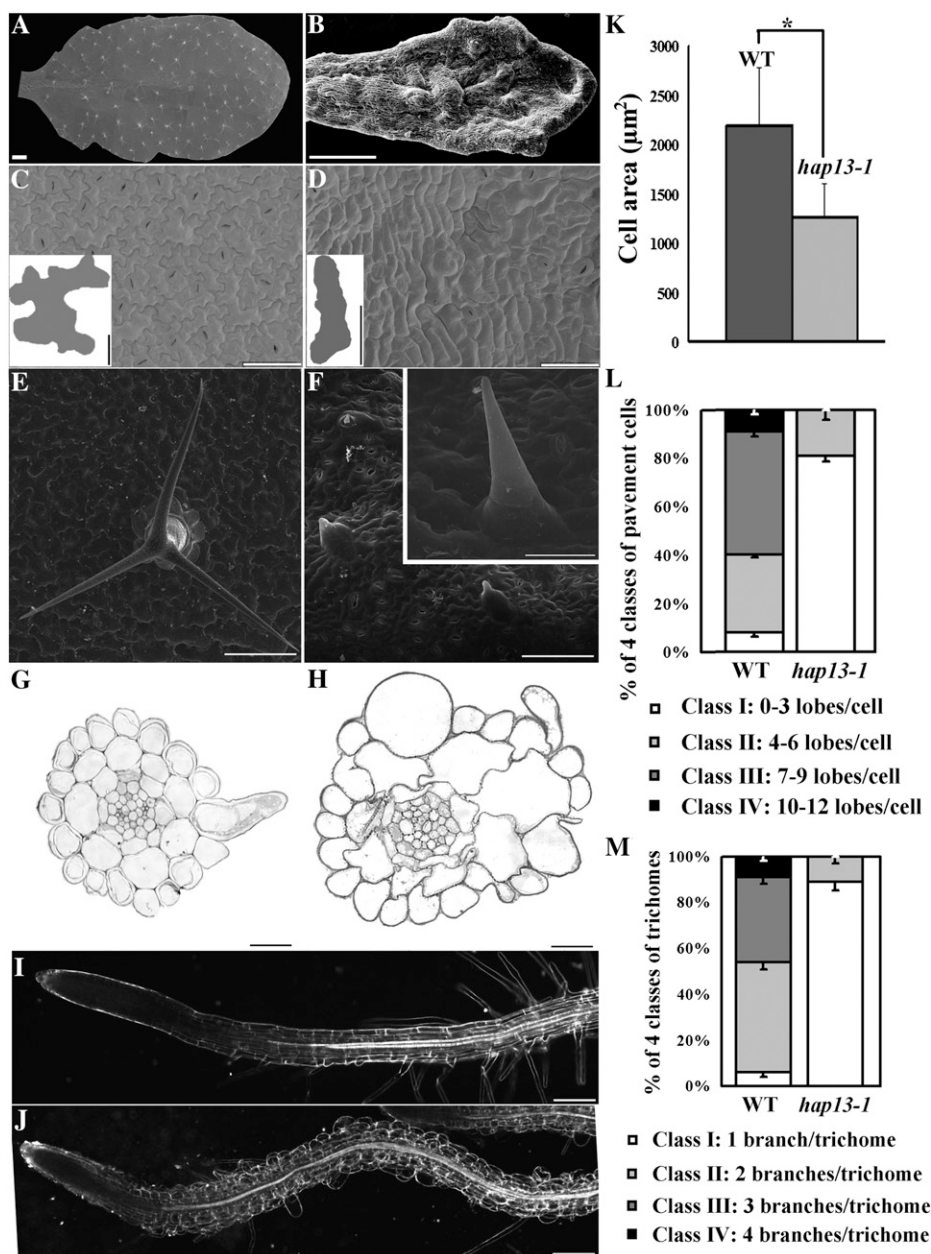
Figure 5. *HAP13* is critical for cell morphogenesis. A to F, Representative scanning electron micrographs of the adaxial surface of leaves from 25-DAG wild-type (A, C, and E) and *hap13-1* (B, D, and F) plants. A and B, Leaf shape in the wild type (A) and *hap13-1* (B). C and D, Closeups of the wild type (C) and *hap13-1* (D) to show pavement cells; example shapes are illustrated in the insets. E and F, Representative trichomes of the wild type (E) and *hap13-1* (F). The inset in F shows a mature trichome of *hap13-1*. G and H, Transverse sections of wild-type (G) and *hap13-1* (H) roots at the root hair elongation zone. I and J, Dark-field images of wild-type (I) and *hap13-1* (J) roots. K to M, Pavement cell size (K), pavement cell complexity (L), and branch number of trichomes (M) are significantly reduced in *hap13-1* (Student's *t* test, *P* < 0.001). Data were collected from seven mature leaves on which 45 to 57 pavement cells or 23 to 33 trichomes were measured for each leaf sample. Results shown in K to M are given as means ± SE. WT, Wild type. Bars = 2 mm for A and B, 50 μm for C and D, 10 μm for C and D insets, 200 μm for E and F, 100 μm for F inset, 20 μm for G and H, and 200 μm for I and J.

Evolutionarily Conserved Localization and Function of HAP13

To confirm that the observed defects were indeed due to functional disruption of *HAP13*, we introduced a GFP translational fusion of the *HAP13* genomic fragment into *hap13-1* (Supplemental Methods S1; Supplemental Table S2). Transcript and phenotypic analyses showed that exogenous *HAP13* fully rescued the defects of *hap13-1* (Fig. 2B; Supplemental Fig. S5), confirming that the phenotypes were due to the mutation in *HAP13*.

Because the GFP translational fusion did not interfere with the function of HAP13, it was used to determine the subcellular localization of HAP13. Consistent

with what was reported recently (Park et al., 2013; Teh et al., 2013), stable transgenic plants expressing 35S: HAP13-red fluorescent protein (RFP) showed punctate vesicles that were sensitive to BFA but not to wortmannin (Supplemental Fig. S5), confirming its identity as the TGN/EE.

To further confirm that HAP13 is the bona fide μ-subunit of AP-1, we introduced *HAP13* into the yeast (*Schizosaccharomyces pombe*) *amp1⁻* mutant (Supplemental Methods S1) in which the μ-subunit of AP-1 was nonfunctional (Kita et al., 2004). *HAP13* complemented the vacuolar fusion defect of the yeast *amp1⁻* mutant upon osmotic stress, albeit to a lesser extent than by *AMP1* (Supplemental Fig. S6), further proving HAP13 as the μ-adaptin of AP-1.
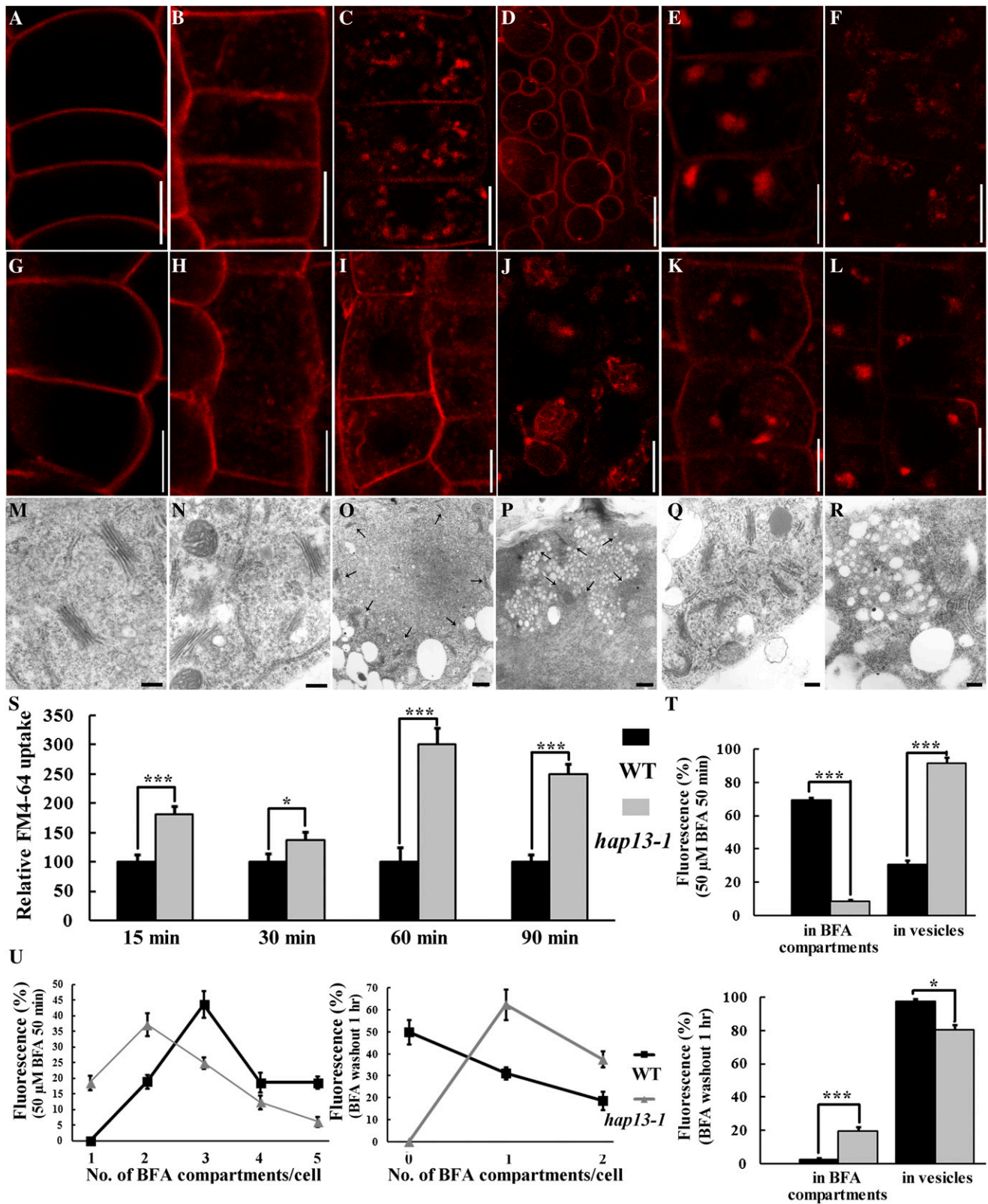
Figure 6. *HAP13* is essential for BFA-sensitive post-Golgi trafficking. A to D, Epidermal cells of 4-DAG wild-type roots were pulse labeled with 4 μM FM4-64 and incubated in MS medium for 1 min (A), 15 min (B), 90 min (C), or 3 h (D) before visualization. E and F, Epidermal cells of 4-DAG wild-type roots were pulse labeled with 4 μM FM4-64 and incubated in MS medium supplemented with BFA for 50 min before imaging (E). BFA washout followed by 1 h of incubation in MS medium is

HAP13 Is Critical for Protein Sorting at the TGN/EE

To determine which trafficking routes are regulated by *HAP13*, we first used the endocytic tracer FM4-64 in an uptake study. Pulse-labeled FM4-64 entered into cells via endocytic trafficking and finally reached the vacuolar membrane (the tonoplast) in the wild type (Fig. 6, A–D), as reported (Feraru et al., 2010). FM4-64 entry from the PM was significantly increased in *hap13-1* (Fig. 6, G, H, and S) at various time points, as represented by the number of endosomes (Fig. 6S). Treatment with 50 µM BFA resulted in intracellular aggregation of FM4-64 signals in the wild type (Fig. 6E), while BFA washout redistributed FM4-64 from the intracellular aggregates (BFA compartments) to endosomes (Fig. 6F). By contrast, a significantly larger amount of the FM4-64 signal remained at endosomes upon BFA treatment in *hap13-1* (Fig. 6, K, T, and U), suggesting reduced sensitivity to BFA. BFA compartments in *hap13-1* were fewer and smaller (Fig. 6, K and T). A large amount of the FM4-64 signal was still enclosed in BFA compartments beside endosome signals upon BFA washout (Fig. 6, L, T, and U).

To confirm the results obtained with FM4-64 uptake, we also performed an ultrastructural study using TEM. No difference regarding the distribution of Golgi and its associated vesicles was obvious in root epidermal cells of the wild type (Fig. 6M) and *hap13-1* (Fig. 6N). BFA treatment induced aggregates of small vesicles that were surrounded with numerous Golgi in the wild type (Fig. 6O). By contrast, aggregates in *hap13-1* were smaller and more irregular (Fig. 6P). In addition, individual vesicles within the aggregates were larger in *hap13-1* (Fig. 6P) than in the wild type (Fig. 6O) upon BFA treatment. BFA washout redistributed vesicles from the BFA compartments, accompanied by randomly redistributed Golgi in the wild type (Fig. 6Q). However, the aggregates in *hap13-1* were insensitive to BFA washout (Fig. 6R). In addition, individual vesicles within the BFA compartments were enlarged in *hap13-1* (Fig. 6R). These results suggested that *HAP13* is critical for BFA-sensitive post-Golgi trafficking from the TGN/EE to the PVC/MVB.

At 3 h, FM4-64 reaches the tonoplast. However, the morphology of the tonoplast seemed irregular in *hap13-1* (Fig. 6J) relative to that in the wild type (Fig. 6D). Therefore, we introduced a fluorescent tonoplast marker, WAVE9R (Geldner et al., 2009), into *hap13-1* to assess this apparent irregularity. Root cells of the wild type contained gradually maturing vacuoles in the root tip to the root hair elongation zone, where a fully expanded central vacuole occupied the entire cell (Supplemental Fig. S7). By contrast, numerous smaller vacuoles were still present in differentiated cells in *hap13-1* (Supplemental Fig. S7), suggesting defective vacuolar fusion.

To further dissect vesicle trafficking routes in which *HAP13* plays critical roles, we introduced fluorescent protein fusions of potential cargos in *hap13-1* and analyzed their dynamic subcellular distribution. BRASSINOSTEROID INSENSITIVE1 (BRI1) is an RLK distributed at the PM and at punctate vesicles in the wild type (Fig. 7A) due to its constitutive endocytic recycling (Russinova et al., 2004). In comparison, a higher percentage of BRI1 signals were detected as punctate vesicles in *hap13-1* (Fig. 7D) than in the wild type (Fig. 7A). BFA together with the protein synthesis inhibitor cycloheximide (CHX) caused an aggregation of BRI1-yellow fluorescent protein (YFP) to the BFA compartments in the wild type (Fig. 7B) and in *hap13-1* (Fig. 7E). Washout of BFA in the presence of CHX relocated BRI1 from the BFA compartments to the PM and punctate vesicles in the wild type (Fig. 7C). By contrast, a higher percentage of BRI1 signals were still present in the BFA compartments and in the cytoplasm in *hap13-1* after BFA washout (Fig. 7F), while they were hardly detected at the PM (Fig. 7F). These results suggested that BFA-sensitive recycling of BRI1-YFP from the TGN/EE to the PM requires *HAP13* function.

We next analyzed the localization of PIN2:GFP (Xu and Scheres, 2005), since PIN2 is critical for gravitropic responses (Paciorek et al., 2005; Abas et al., 2006) and gravitropism was compromised in *hap13-1*. PIN2:GFP was distributed asymmetrically in the epidermal cells of wild-type roots (Fig. 7G) as reported (Paciorek et al., 2005; Xu and Scheres, 2005; Jaillais et al., 2006; Dhonukshe et al., 2007; Wang et al., 2013). By contrast, the distribution of PIN2:GFP in *hap13-1* was irregular at the PM (Fig. 7J). BFA together with CHX induced the aggregation of PIN2 to BFA compartments in both the wild type and

Figure 6. (*Continued.*)
shown in F. G to J, Epidermal cells of 4-DAG *hap13-1* roots were pulse labeled with 4 µM FM4-64 and incubated in MS medium for 1 min (G), 15 min (H), 90 min (I), and 3 h (J) before visualization. K and L, Epidermal cells of 4-DAG *hap13-1* roots were pulse-labeled with 4 µM FM4-64 and incubated in MS medium supplemented with BFA for 50 min before imaging (K). BFA washout followed by 1 h of incubation in MS medium is shown in L. M to R, TEM of wild-type (M, O, and Q) and *hap13-1* (N, P, and R) root epidermal cells under control conditions (M and N), treated with 50 µM BFA for 50 min (O and P), or treated with BFA followed by a 1-h washout (Q and R). Arrows in O and P indicate the Golgi apparatus surrounding the BFA compartment. S to U, Quantification of FM4-64 uptake (S), percentage of fluorescence distribution (T), and number of BFA compartments (U) either upon BFA treatment (50 µM for 50 min) or after BFA washout (1 h). Data were collected from nine optical sections of roots in which six to eight cells in each optical section were used to calculate the areas of fluorescence or the number of punctate vesicles with ImageJ. Results shown in S to U are given as means ± SE. Asterisks represent significant differences (Student's *t* test, *$P < 0.01$ or ***$P < 0.001$). Nonbiased double-blind analyses were conducted to confirm the differences between the wild type (WT) and *hap13-1*. Bars = 7.5 µm for A to L, 200 nm for M, N, Q, and R, and 500 nm for O and P. [See online article for color version of this figure.]

Figure 7. HAP13 is critical for trans-membrane cargo sorting at the TGN/EE. A to F, BRI1:YFP (false-colored green) in the wild type (A–C) or hap13-1 (D–F). Control images (A and D) were taken before roots were treated with MS medium supplemented with 50 μM BFA and 50 μM CHX for 50 min in the wild type (B) or hap13-1 (E). After BFA washout, roots were further incubated with MS medium supplemented with 50 μM CHX for 1 h in the wild type (C) or hap13-1 (F). G to L, PIN2:GFP in the wild type (G–I) or hap13-1 (J–L). Control images (G and J) were taken before roots were treated with MS medium supplemented with 50 μM BFA and 50 μM CHX for 50 min in the wild type (H) or hap13-1 (K). After BFA washout, roots were further incubated with MS medium supplemented with 50 μM CHX for 1 h in the wild type (I) or hap13-1 (L). Bars = 5 μm for A to F and 7.5 μm for G to L. [See online article for color version of this figure.]
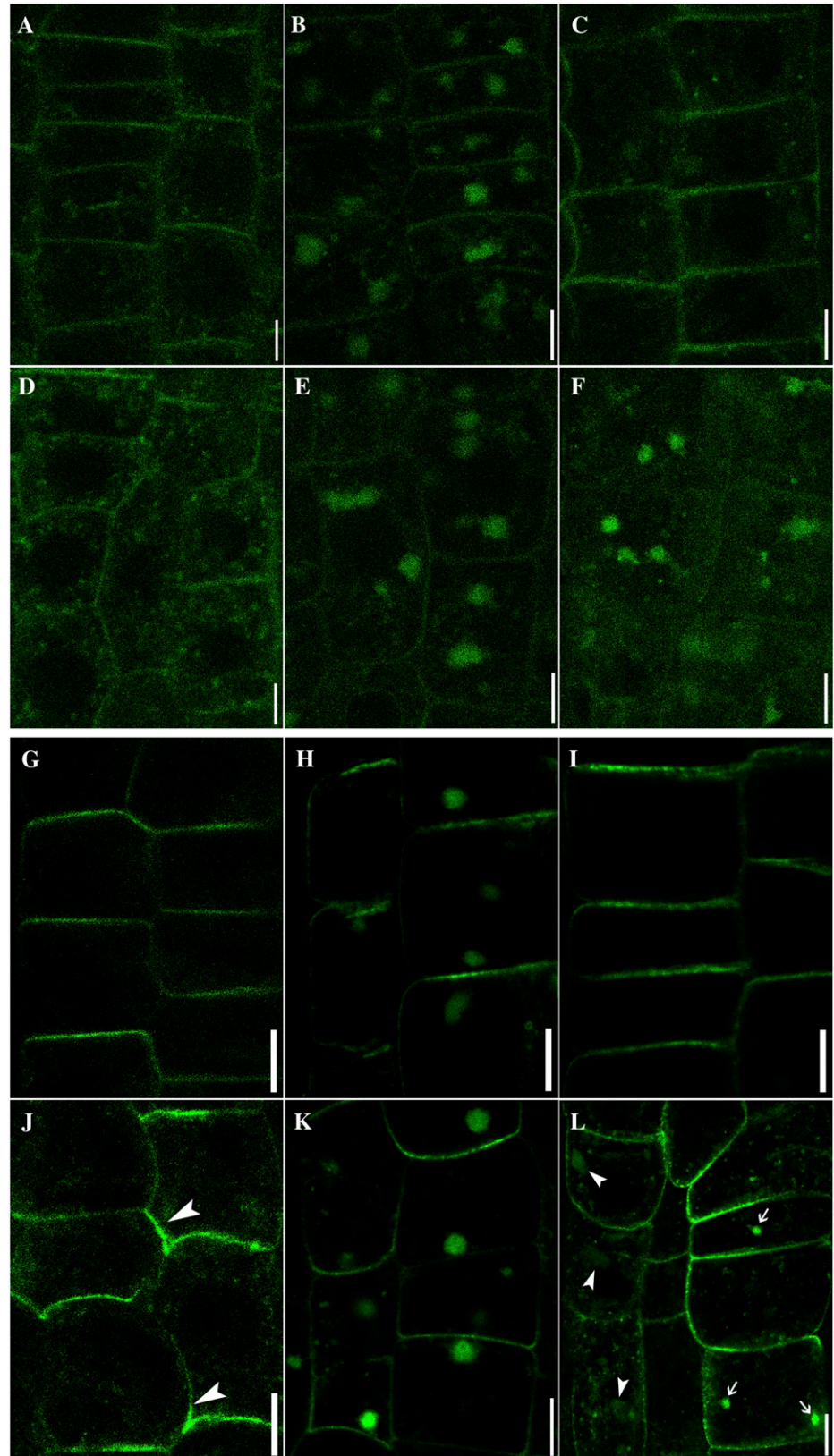
hap13-1 (Fig. 7, H and K). However, a portion of the PIN2 signal was still detected at punctate vesicles in *hap13-1* (Fig. 7K), suggesting hyposensitivity to BFA. BFA washout in the presence of CHX relocated PIN2 to the PM in the wild type (Fig. 7I). By contrast, a large fraction of signals were detected at punctate vesicles as well as vacuoles in *hap13-1* after BFA washout (Fig. 7L). These results suggested that the asymmetric localization of PIN2 at the PM through recycling from the TGN/EE requires *HAP13*.

DISCUSSION

HAP13 Is the Arabidopsis μ1 Adaptin Regulating Diverse Developmental and Cellular Processes

The Arabidopsis genome encodes components for all five AP complexes (Boehm and Bonifacino, 2001; Holstein, 2002; Hirst et al., 2011). However, functional characterization of AP complexes was scarce. Pharmacological treatment with tyrphostin A23, a specific inhibitor for AP-2-mediated receptor internalization, inhibited the endocytosis of PM proteins in plant cells (Ortiz-Zapater et al., 2006; Dhonukshe et al., 2007), suggesting the presence of AP-2. Earlier studies showed that Arabidopsis μA adaptin interacted with a peptide with tandem Tyr-based motifs from a pea (*Pisum sativum*) vacuolar sorting receptor (Happel et al., 2004). Arabidopsis AP-3 mediates the biogenesis and function of lytic vacuoles and is insensitive to BFA and wortmannin (Feraru et al., 2010; Zwiewka et al., 2011), similar to AP-3s of other phyla.

The function of AP-1 was suggested earlier by the identification of the rice (*Oryza sativa*) mutant *spl28*, which resulted in a C-terminal truncation of SPL28, a protein homologous to μ1 adaptins (Qiao et al., 2010). However, SPL28 was localized at the Golgi in a transient assay (Qiao et al., 2010), casting doubt on its roles as a component of the AP-1 complex. However, two recent papers published during the preparation of this article reported that HAP13/AP1M2 is the major Arabidopsis μ1 adaptin (Park et al., 2013; Teh et al., 2013). By using biochemical and cellular approaches, they both showed that HAP13/AP1M2 was localized at the TGN and formed a complex with other components of AP-1, conforming to its evolutionarily conserved characteristics as a μ1 adaptin (Park et al., 2013; Teh et al., 2013).

Our results reported here demonstrate that AP-1, presumably through intracellular protein sorting at the TGN/EE, influences a full spectrum of developmental and cellular processes. We show that HAP13 is critical for Arabidopsis viability (Fig. 2) in almost all aspects of plant development (Figs. 2 and 3) and cell morphogenesis (Fig. 5), consistent with the key roles of AP-1 in other multicellular organisms (Meyer et al., 2000; Boehm and Bonifacino, 2001). HAP13 associates with BFA-sensitive but wortmannin-insensitive endosomes suggestive of the TGN/EE (Supplemental Fig. S5), as confirmed recently (Park et al., 2013). Based on FM4-64 labeling (Fig. 6) as well as the localization pattern of a fluorescent probe for the tonoplast (Supplemental Fig. S7), we found that fully differentiated cells in *hap13-1* contained fragmented vacuoles rather than a large central vacuole as in the wild type, suggesting defective vacuolar fusion similar to that observed in the yeast μ1 mutant (Kita et al., 2004). One of the two recent publications on *HAP13* concluded that there was no discernible defect in vacuolar morphology, based on a 5-h FM4-64 uptake study (Park et al., 2013). However, vacuoles mature progressively during root development (Supplemental Fig. S7). Therefore, the morphology of vacuoles depends greatly on the positions of cells in roots. Capturing vacuoles from various developmental stages (Supplemental Fig. S7) would be needed to conclude whether vacuolar morphology was affected in a given mutant. Indeed, exogenous *HAP13* did restore the vacuole fusion of the yeast *amp1⁻* (Supplemental Fig. S6), supporting its evolutionarily conserved roles. Finally, we show that intracellular sorting of transmembrane cargos, either the auxin efflux carrier PIN2 or the brassinosteroid receptor BRI1, is compromised in *hap13-1* (Fig. 7), correlating with the critical role of AP-1 in intracellular protein sorting. However, it is worthy of note that BFA caused the AP-1 complex to become cytosolic in metazoa (Waguri et al., 2003), but HAP13 aggregated into the BFA compartments upon BFA treatment rather than becoming cytosolic (Supplemental Fig. S5). That may suggest phylum-specific localization mechanisms for AP-1.

HAP13 Regulates Endomembrane Trafficking

The recent progress on AP-1 in Arabidopsis showed that HAP13/AP1M2 is essential for the intracellular trafficking of KNOLLE, leading to defects in cytokinesis (Park et al., 2013; Teh et al., 2013). Our results demonstrated that vesicle trafficking centered on the TGN/EE was in general compromised in *hap13-1*.

First, the endocytic trafficking of FM4-64 from the PM to the TGN/EE was enhanced in *hap13-1*, supported by a nonbiased double-blind quantitative analysis (Fig. 6). Although Park et al. (2013) reported that no difference was observed for the endocytosis of FM4-64 between the wild type and *hap13-1*, the time point on which that conclusion was based was 5 min, which might be too short a period for detectable differences. Instead, we followed FM4-64 uptake qualitatively and quantitatively from 15 min to 3 h (Fig. 6). The increased endocytosis is intriguing, considering that genetically interfering with the formation of clathrin-coated vesicles (CCVs) resulted in defective uptake of FM4-64 as well as compromised internalization of PM proteins (Dhonukshe et al., 2007; Kitakura et al., 2011; Wang et al., 2013). On the other hand, both AP-1 and AP-2 complexes recruit clathrin during the formation of CCVs but at different intracellular localizations (Robinson, 2004). Therefore, it is likely that more CCVs would be allocated to the PM in *hap13-1*, leading to the increased internalization rate. Indeed,

HAP13 was present in the same complex as CCV components (Park et al., 2013). Furthermore, a deficiency of μ1A in fibroblasts induced an increased internalization of a μ1A cargo receptor (Meyer et al., 2001), suggesting that AP-1-mediated transport of that receptor at the TGN did influence its internalization from the PM.

Second, recycling of internalized proteins from the TGN/EE to the PM was compromised in *hap13-1* (Fig. 7). For example, the asymmetric localization of PIN2 (Paciorek et al., 2005; Jaillais et al., 2006; Dhonukshe et al., 2007; Kitakura et al., 2011; Wang et al., 2013) was compromised, and recycling of PIN2 to the PM after BFA washout was inhibited in *hap13-1* (Fig. 7), consistent with what's been reported recently (Park et al., 2013). Similar observations were reported when mutations disrupted the function of ArfGEFs, the cellular targets of BFA (Geldner et al., 2003; Xu and Scheres, 2005; Richter et al., 2007; Teh and Moore, 2007). The essential roles of ArfGEFs in regulating post-Golgi trafficking (Geldner et al., 2003; Richter et al., 2007; Teh and Moore, 2007; Tanaka et al., 2009) have been extensively characterized. For example, GNOM-LIKE1 plays an evolutionarily conserved role at the Golgi (Richter et al., 2007; Teh and Moore, 2007), while the other two ArfGEFs, GNOM and BEN1 (for BFA-visualized endocytic trafficking defective1), function at recycling endosomes (Geldner et al., 2003; Richter et al., 2007) and the TGN (Tanaka et al., 2009), respectively. In mammalian cells, the association of AP-1 at the TGN requires Arf1 activation by ArfGEFs (Heldwein et al., 2004). Considering the resemblance of defects in intracellular protein sorting, it is likely that ArfGEFs may regulate the TGN/EE association of HAP13. Cargos destined for the recycling route were proposed to pass BEN1-positive endosomes and further transported to the GNOM-positive RE to deliver to the PM (Tanaka et al., 2009). It is interesting that a similar scenario was proposed in mammalian cells, in which two types of mammalian AP-1 (A and B) are present in distinct endosome populations (i.e. the TGN and the RE; Gonzalez and Rodriguez-Boulan, 2009). Such similarity hints at the intriguing possibility that Arabidopsis HAP13 performs dual roles at the BEN1-positive TGN and the GNOM-positive RE for protein sorting to the recycling route, in which HAP13 needs to be regulated in a location-sensitive manner for its cargo specificity. However, despite their apparent redundancy, the recently identified HAP13 homolog, AP1M1 (Park et al., 2013), may provide an alternative scenario that waits to be explored.

Finally, our results also hinted at the possibility that HAP13 is critical for trafficking from the TGN/EE via the PVC/MVB to the vacuole. FM4-64 did reach the tonoplast after 3 h of uptake, indicating that there are at least some trafficking routes proceeding from the TGN/EE to the vacuole in the mutant. However, upon BFA washout, FM4-64 signals were largely retained in the BFA compartments in *hap13-1* rather than going through the PVC/MVB to reach the tonoplast in the

wild type (Fig. 6). In addition, the distribution pattern of FM4-64 after 3 h of uptake was fragmented and irregular (Fig. 6). Fluorescent labeling with WAVE9R also confirmed the defects of vacuolar morphology in *hap13-1* (Supplemental Fig. S7), suggesting that vacuolar transport of some cargos was defective. Indeed, Park et al. (2013) showed biochemically that some soluble vacuolar proteins failed to reach the vacuole in the mutant. Furthermore, dark-induced vacuolar delivery of PIN2 was compromised in the mutant of *HAP13*, which also suggested defective vacuolar trafficking.

Taken together, our results and those of others (Park et al., 2013; Teh et al., 2013) demonstrate that HAP13 is critical for protein sorting centered on the TGN/EE.

HAP13 Regulates Development and Cell Morphogenesis through Cargo Sorting

The pleiotropic developmental and cellular defects shown by *hap13-1* suggest tissue- and cell-specific cargo proteins. The pleiotropic developmental defects of *hap13-1* (Figs. 2 and 3) were attributed partially to disturbed auxin signaling (Blilou et al., 2005; Abas et al., 2006; Dhonukshe et al., 2008; Rosado et al., 2010). The auxin maximum (Ulmasov et al., 1997) and polar localization of PIN2 are disrupted in *hap13-1* (Figs. 4 and 7). It was recently shown that dynamic and polar localization of PINs regulated by auxin plays a critical role in the interdigitation of leaf pavement cells (Robert et al., 2010). Although we did not examine the localization pattern of other PINs in leaf cells, the disrupted localization of PIN2 in *hap13-1* (Fig. 7) suggests a similar situation in other cell types. A YXXϕ motif has been identified in the cytosolic loop of all PINs (Mravec et al., 2009). However, no functional relevance has been assigned to this motif.

In addition to PIN-driven auxin gradients, RLKs play critical roles in a full spectrum of plant growth, such as plant height, leaf size, inflorescence architecture, vascular development, as well as root growth (De Smet et al., 2009). A large number of RLKs contain sorting motifs recognizable by the AP complexes, and endocytic trafficking of some RLKs has been reported (Geldner and Robatzek, 2008; Irani and Russinova, 2009). However, little information is available on the importance of such motifs in intracellular sorting. We demonstrated that the brassinosteroid receptor BRI1 was mislocalized in *hap13-1*, as a result of disrupted recycling from the TGN/EE (Fig. 7). Considering the importance of brassinosteroid receptor signaling in plants (Wang et al., 2001), it is not surprising that pleiotropic developmental defects were observed in *hap13-1* (Fig. 2).

Considering the severe defects both in developmental aspects and in cell morphogenesis in *hap13-1*, further efforts by whole-genome and proteomic approaches to identify cargo proteins subjected to intracellular sorting through μ1 will yield important insights not only

into vesicle trafficking routes mediated by AP-1 in particular but also into the mechanisms of cell and organ morphogenesis in general.

MATERIALS AND METHODS

Plant Materials and Growth Conditions

Arabidopsis (*Arabidopsis thaliana*) *hap13* (CS16318) and *hap13-2* (SALK_024181) were obtained from the Arabidopsis Biological Resource Center. *hap13-1* (FLAG_293C11) was obtained from the Institut National de la Recherche Agronomique. Arabidopsis ecotype Columbia or Wassilewskija (Ws) was used as the wild type. Plants were grown as described (Zhou et al., 2013).

Analysis of Auxin Distribution and Responses

hap13-1 was crossed with *Pro_{DR5}*:GUS and *Pro_{DR5}*:GFP (Ulmasov et al., 1997) to determine auxin distribution patterns. GUS staining were performed with 5- to 8-DAG seedlings of *Pro_{DR5}*:GUS;Ws or *Pro_{DR5}*:GUS;*hap13-1*. Gravitropic responses of primary roots were measured as described (Abas et al., 2006). Amyloplast deposition in root tips by Lugol's staining was performed as described (Kitakura et al., 2011). FM4-64 was pulse labeled to delineate root cells of 5-DAG seedlings of *Pro_{DR5}*:GFP;Ws or *Pro_{DR5}*:GFP;*hap13-1*.

Phenotype Analysis

For venation pattern imaging, leaves of the wild type and *hap13-1* at 25 DAG were fixed for 1 h in acetic acid:95% ethanol (1:3), cleared in a sequential ethanol series, and finally fixed in 10% NaOH for 1 h at 42°C. Specimens were mounted on slides in 50% glycerol and visualized with a Zeiss Axiophot microscope under dark-field illumination. Vascular development of roots, stems, and inflorescence stems was determined as described (Cnops et al., 2006). Scanning electron microscopy and TEM were performed as described (Zhou et al., 2013).

Pharmacological Treatments

For FM4-64 uptake, roots of 4- to 5-DAG seedlings were pulse labeled with 4 μM FM4-64 for 5 min except for the 1-min assay. Roots were then taken out, washed three times with liquid MS medium without FM4-64, and visualized for FM4-64 intake at designated times. For BFA (Sigma; 50 μM in dimethyl sulfoxide) treatment of FM4-64 labeling, roots were pulse labeled with FM4-64 for 5 min, washed and incubated with MS medium supplemented with 50 μM BFA for 50 min, and visualized for the formation of BFA compartments. BFA washout was performed by washing the above seedlings with MS medium without BFA three times before further incubation. BFA treatment and washout for roots expressing BRI1:YFP and PIN2:GFP were performed similarly except that both BFA treatment and washout were performed in the presence of 50 μM CHX. Wortmannin treatment was performed as described (Jaillais et al., 2006).

Microscopy and Fluorescence Signal Quantification

Transgenic plants of *Pro_{HAP13}*:NLS-YFP and sections were captured using Axio Observer D1 equipped with a CCD camera (Zeiss). Other fluorescent images were captured by an inverted laser scanning confocal microscope (LSM780; Zeiss) with a Plan-Neofluar ×40/1.3 oil differential interference contrast objective or ×63/1.45 oil differential interference contrast objective. TEM was performed as described (Li et al., 2013). GFP-RFP double-labeled plant materials were captured alternately using line switching with the multi-track function (488 nm for GFP and 545 nm for RFP). Fluorescence was detected using a 505- to 550-nm band-pass filter for GFP and a 575- to 650-nm band-pass filter for RFP. Postacquisition image processing was performed with the LSM image-processing software (Zeiss). For quantification of FM4-64 uptake from 15 to 90 min, vesicles in the cytoplasm of 60 to 72 root epidermal cells were counted with ImageJ (http://rsbweb.nih.gov/ij/). For quantification of FM4-64 agglomeration upon BFA treatment and after BFA washout, FM4-64 agglomerations were counted with ImageJ. Data were collected from 54 to 63 root epidermal cells for each genotype.

Sequence data from this article can be found in The Arabidopsis Information Resource database under accession number At1g60780 (*HAP13*).

Supplemental Data

The following materials are available in the online version of this article.

Supplemental Figure S1. Germination of *hap13-1* pollen was significantly reduced.

Supplemental Figure S2. *hap13-1* showed reduced growth of primary roots but enhanced initiation of lateral roots.

Supplemental Figure S3. *hap13-1* showed enhanced ROS production and cell death in leaves.

Supplemental Figure S4. Vascular development was defective in leaves but not in roots or hypocotyls in *hap13-1*.

Supplemental Figure S5. A GFP translational fusion of *HAP13* fully rescued the growth defects of *hap13-1*.

Supplemental Figure S6. *HAP13* complemented the defective vacuolar fusion of the yeast *apm1⁻* mutant upon osmotic stresses.

Supplemental Figure S7. *hap13-1* showed defective vacuolar fusion.

Supplemental Table S1. Mutations at *HAP13* resulted in defective male transmission.

Supplemental Table S2. Oligonucleotides used in this study.

Supplemental Methods S1.

LITERATURE CITED

Abas L, Benjamins R, Malenica N, Paciorek T, Wiśniewska J, Moulinier-Anzola JC, Sieberer T, Friml J, Luschnig C (2006) Intracellular trafficking and proteolysis of the *Arabidopsis* auxin-efflux facilitator PIN2 are involved in root gravitropism. Nat Cell Biol **8:** 249–256

Altamura MM, Possenti M, Matteucci A, Baima S, Ruberti I, Morelli G (2001) Development of the vascular system in the inflorescence stem of *Arabidopsis*. New Phytol **151:** 381–389

Blilou I, Xu J, Wildwater M, Willemsen V, Paponov I, Friml J, Heidstra R, Aida M, Palme K, Scheres B (2005) The PIN auxin efflux facilitator network controls growth and patterning in *Arabidopsis* roots. Nature **433:** 39–44

Boehm M, Bonifacino JS (2001) Adaptins: the final recount. Mol Biol Cell **12:** 2907–2920

Cnops G, Neyt P, Raes J, Petrarulo M, Nelissen H, Malenica N, Luschnig C, Tietz O, Ditengou F, Palme K, et al (2006) The *TORNADO1* and *TORNADO2* genes function in several patterning processes during early leaf development in *Arabidopsis thaliana*. Plant Cell **18:** 852–866

De Marcos Lousa C, Gershlick DC, Denecke J (2012) Mechanisms and concepts paving the way towards a complete transport cycle of plant vacuolar sorting receptors. Plant Cell **24:** 1714–1732

De Smet I, Voss U, Jürgens G, Beeckman T (2009) Receptor-like kinases shape the plant. Nat Cell Biol **11:** 1166–1173

Dettmer J, Hong-Hermesdorf A, Stierhof YD, Schumacher K (2006) Vacuolar H⁺-ATPase activity is required for endocytic and secretory trafficking in *Arabidopsis*. Plant Cell **18:** 715–730

Dhonukshe P, Aniento F, Hwang I, Robinson DG, Mravec J, Stierhof YD, Friml J (2007) Clathrin-mediated constitutive endocytosis of PIN auxin efflux carriers in *Arabidopsis*. Curr Biol **17:** 520–527

Dhonukshe P, Tanaka H, Goh T, Ebine K, Mähönen AP, Prasad K, Blilou I, Geldner N, Xu J, Uemura T, et al (2008) Generation of cell polarity in plants links endocytosis, auxin distribution and cell fate decisions. Nature **456:** 962–966

Ebine K, Ueda T (2009) Unique mechanism of plant endocytic/vacuolar transport pathways. J Plant Res **122:** 21–30

Feraru E, Paciorek T, Feraru MI, Zwiewka M, De Groodt R, De Rycke R, Kleine-Vehn J, Friml J (2010) The AP-3 β adaptin mediates the biogenesis and function of lytic vacuoles in *Arabidopsis*. Plant Cell **22:** 2812–2824

Geldner N, Anders N, Wolters H, Keicher J, Kornberger W, Muller P, Delbarre A, Ueda T, Nakano A, Jürgens G (2003) The *Arabidopsis* GNOM ARF-GEF mediates endosomal recycling, auxin transport, and auxin-dependent plant growth. Cell **112:** 219–230

Geldner N, Dénervaud-Tendon V, Hyman DL, Mayer U, Stierhof YD, Chory J (2009) Rapid, combinatorial analysis of membrane compartments in intact plants with a multicolor marker set. Plant J **59:** 169–178

Geldner N, Robatzek S (2008) Plant receptors go endosomal: a moving view on signal transduction. Plant Physiol **147:** 1565–1574

Gonzalez A, Rodriguez-Boulan E (2009) Clathrin and AP1B: key roles in basolateral trafficking through trans-endosomal routes. FEBS Lett **583:** 3784–3795

Happel N, Höning S, Neuhaus JM, Paris N, Robinson DG, Holstein SE (2004) Arabidopsis mu A-adaptin interacts with the tyrosine motif of the vacuolar sorting receptor VSR-PS1. Plant J **37:** 678–693

Heldwein EE, Macia E, Wang J, Yin HL, Kirchhausen T, Harrison SC (2004) Crystal structure of the clathrin adaptor protein 1 core. Proc Natl Acad Sci USA **101:** 14108–14113

Hirst J, Barlow LD, Francisco GC, Sahlender DA, Seaman MN, Dacks JB, Robinson MS (2011) The fifth adaptor protein complex. PLoS Biol **9:** e1001170

Holstein SE (2002) Clathrin and plant endocytosis. Traffic **3:** 614–620

Huang F, Nesterov A, Carter RE, Sorkin A (2001) Trafficking of yellow-fluorescent-protein-tagged mu1 subunit of clathrin adaptor AP-1 complex in living cells. Traffic **2:** 345–357

Irani NG, Russinova E (2009) Receptor endocytosis and signaling in plants. Curr Opin Plant Biol **12:** 653–659

Jaillais Y, Fobis-Loisy I, Miège C, Rollin C, Gaude T (2006) AtSNX1 defines an endosome for auxin-carrier trafficking in *Arabidopsis*. Nature **443:** 106–109

Johnson MA, von Besser K, Zhou Q, Smith E, Aux G, Patton D, Levin JZ, Preuss D (2004) Arabidopsis *hapless* mutations define essential gametophytic functions. Genetics **168:** 971–982

Kita A, Sugiura R, Shoji H, He Y, Deng L, Lu Y, Sio SO, Takegawa K, Sakaue M, Shuntoh H, et al (2004) Loss of Apm1, the micro1 subunit of the clathrin-associated adaptor-protein-1 complex, causes distinct phenotypes and synthetic lethality with calcineurin deletion in fission yeast. Mol Biol Cell **15:** 2920–2931

Kitakura S, Vanneste S, Robert S, Löfke C, Teichmann T, Tanaka H, Friml J (2011) Clathrin mediates endocytosis and polar distribution of PIN auxin transporters in *Arabidopsis*. Plant Cell **23:** 1920–1931

Kleine-Vehn J, Leitner J, Zwiewka M, Sauer M, Abas L, Luschnig C, Friml J (2008) Differential degradation of PIN2 auxin efflux carrier by retromer-dependent vacuolar targeting. Proc Natl Acad Sci USA **105:** 17812–17817

Lam SK, Siu CL, Hillmer S, Jang S, An G, Robinson DG, Jiang L (2007) Rice SCAMP1 defines clathrin-coated, *trans*-Golgi-located tubular-vesicular structures as an early endosome in tobacco BY-2 cells. Plant Cell **19:** 296–319

Li S, Ge FR, Xu M, Zhao XY, Huang GQ, Zhou LZ, Wang JG, Kombrink A, McCormick S, Zhang XS, et al (2013) Arabidopsis COBRA-LIKE 10, a GPI-anchored protein, mediates directional growth of pollen tubes. Plant J **74:** 486–497

Meyer C, Eskelinen EL, Guruprasad MR, von Figura K, Schu P (2001) Mu 1A deficiency induces a profound increase in MPR300/IGF-II receptor internalization rate. J Cell Sci **114:** 4469–4476

Meyer C, Zizioli D, Lausmann S, Eskelinen EL, Hamann J, Saftig P, von Figura K, Schu P (2000) Mu1A-adaptin-deficient mice: lethality, loss of AP-1 binding and rerouting of mannose 6-phosphate receptors. EMBO J **19:** 2193–2203

Mravec J, Skůpa P, Bailly A, Hoyerová K, Krecek P, Bielach A, Petrásek J, Zhang J, Gaykova V, Stierhof Y-D, et al (2009) Subcellular homeostasis

of phytohormone auxin is mediated by the ER-localized PIN5 transporter. Nature **459:** 1136–1140

Ortiz-Zapater E, Soriano-Ortega E, Marcote MJ, Ortiz-Masiá D, Aniento F (2006) Trafficking of the human transferrin receptor in plant cells: effects of tyrphostin A23 and brefeldin A. Plant J **48:** 757–770

Paciorek T, Zazímalová E, Ruthardt N, Petrásek J, Stierhof YD, Kleine-Vehn J, Morris DA, Emans N, Jürgens G, Geldner N, et al (2005) Auxin inhibits endocytosis and promotes its own efflux from cells. Nature **435:** 1251–1256

Park M, Song K, Reichardt I, Kim H, Mayer U, Stierhof Y-D, Hwang I, Jürgens G (2013) *Arabidopsis* μ-adaptin subunit AP1M of adaptor protein complex 1 mediates late secretory and vacuolar traffic and is required for growth. Proc Natl Acad Sci USA **110:** 10318–10323

Qiao Y, Jiang W, Lee J, Park B, Choi M-S, Piao R, Woo M-O, Roh J-H, Han L, Paek N-C, et al (2010) SPL28 encodes a clathrin-associated adaptor protein complex 1, medium subunit micro 1 (AP1M1) and is responsible for spotted leaf and early senescence in rice (Oryza sativa). New Phytol **185:** 258–274

Richter S, Geldner N, Schrader J, Wolters H, Stierhof YD, Rios G, Koncz C, Robinson DG, Jürgens G (2007) Functional diversification of closely related ARF-GEFs in protein secretion and recycling. Nature **448:** 488–492

Richter S, Voss U, Jürgens G (2009) Post-Golgi traffic in plants. Traffic **10:** 819–828

Robert S, Kleine-Vehn J, Barbez E, Sauer M, Paciorek T, Baster P, Vanneste S, Zhang J, Simon S, Čovanová M, et al (2010) ABP1 mediates auxin inhibition of clathrin-dependent endocytosis in *Arabidopsis*. Cell **143:** 111–121

Robinson MS (2004) Adaptable adaptors for coated vesicles. Trends Cell Biol **14:** 167–174

Rosado A, Sohn EJ, Drakakaki G, Pan S, Swidergal A, Xiong Y, Kang BH, Bressan RA, Raikhel NV (2010) Auxin-mediated ribosomal biogenesis regulates vacuolar trafficking in *Arabidopsis*. Plant Cell **22:** 143–158

Russinova E, Borst JW, Kwaaitaal M, Caño-Delgado A, Yin Y, Chory J, de Vries SC (2004) Heterodimerization and endocytosis of *Arabidopsis* brassinosteroid receptors BRI1 and AtSERK3 (BAK1). Plant Cell **16:** 3216–3229

Tanaka H, Kitakura S, De Rycke R, De Groodt R, Friml J (2009) Fluorescence imaging-based screen identifies ARF GEF component of early endosomal trafficking. Curr Biol **19:** 391–397

Teh OK, Moore I (2007) An ARF-GEF acting at the Golgi and in selective endocytosis in polarized plant cells. Nature **448:** 493–496

Teh OK, Shimono Y, Shirakawa M, Fukao Y, Tamura K, Shimada T, Hara-Nishimura I (2013) The AP-1 μ adaptin is required for KNOLLE localization at the cell plate to mediate cytokinesis in Arabidopsis. Plant Cell Physiol **54:** 838–847

Ulmasov T, Murfett J, Hagen G, Guilfoyle TJ (1997) Aux/IAA proteins repress expression of reporter genes containing natural and highly active synthetic auxin response elements. Plant Cell **9:** 1963–1971

Viotti C, Bubeck J, Stierhof YD, Krebs M, Langhans M, van den Berg W, van Dongen W, Richter S, Geldner N, Takano J, et al (2010) Endocytic and secretory traffic in *Arabidopsis* merge in the trans-Golgi network/early endosome, an independent and highly dynamic organelle. Plant Cell **22:** 1344–1357

Waguri S, Dewitte F, Le Borgne R, Rouillé Y, Uchiyama Y, Dubremetz JF, Hoflack B (2003) Visualization of TGN to endosome trafficking through fluorescently labeled MPR and AP-1 in living cells. Mol Biol Cell **14:** 142–155

Wang C, Yan X, Chen Q, Jiang N, Fu W, Ma B, Liu J, Li C, Bednarek SY, Pan J (2013) Clathrin light chains regulate clathrin-mediated trafficking, auxin signaling, and development in *Arabidopsis*. Plant Cell **25:** 499–516

Wang Z-Y, Seto H, Fujioka S, Yoshida S, Chory J (2001) BRI1 is a critical component of a plasma-membrane receptor for plant steroids. Nature **410:** 380–383

Xu J, Scheres B (2005) Dissection of *Arabidopsis* ADP-RIBOSYLATION FACTOR 1 function in epidermal cell polarity. Plant Cell **17:** 525–536

Zhou L-Z, Li S, Feng Q-N, Zhang Y-L, Zhao X, Zeng Y, Wang H, Jiang L, Zhang Y (2013) Arabidopsis PROTEIN S-ACYLTRANSFERASE 10 is critical for development and salt tolerance. Plant Cell **25:** 1093–1107

Zwiewka M, Feraru E, Möller B, Hwang I, Feraru MI, Kleine-Vehn J, Weijers D, Friml J (2011) The AP-3 adaptor complex is required for vacuolar function in *Arabidopsis*. Cell Res **21:** 1711–1722